BIOCHEMISTRY
including biophysical chemistry & molecular biology

Article

pubs.acs.org/biochemistry

What Singles Out the G[8−5]C Intrastrand DNA Cross-Link? Mechanistic and Structural Insights from Quantum Mechanics/Molecular Mechanics Simulations

Chandan Patel,[†] Julian Garrec,[‡] Céline Dupont,[†] and Elise Dumont*[,†]

[†]Université de Lyon, Institut de Chimie de Lyon, CNRS, Ecole normale supérieure de Lyon, 46 allée d'Italie, 69364 Lyon Cedex 07, France

[‡]Laboratory of Computational Chemistry and Biochemistry, Institute of Chemical Sciences and Engineering, École Polytechnique Fédérale de Lausanne, CH-1015 Lausanne, Switzerland

Supporting Information

ABSTRACT: Naturally occurring intrastrand oxidative cross-link lesions have proven to be a potent source of endogenous DNA damage. Among the variety of lesions that can be formed and have been identified, G[8−5]C damage (in which the C8 atom of a guanine is covalently bonded to the C5 atom of a nearby cytosine belonging to the same strand) occurs with a low incidence yet takes on special importance because of its high mutagenicity. Hybrid Car−Parrinello molecular dynamics simulations, rooted in density functional theory and coupled to molecular mechanics, have been performed to shed light on the cyclization process. The activation free energy of the reacting subsystem embedded in a solvated dodecamer is estimated to be ∼12.4 kcal/mol, which is ∼3 kcal/mol higher than the value for the prototypical G[8−5m]T lesion inferred employing the same theoretical framework [Garrec, J., Patel, C., Rothlisberger, U., and Dumont, E. (2012) *J. Am. Chem. Soc. 134*, 2111−2119]. This study also situates the G[8−5m]mC lesion at an intermediate activation free energy (∼10.5 kcal/mol). The order of reactivity in DNA (T$^\bullet$ > mC$^\bullet$ > C$^\bullet$) is reversed compared to that in the reacting subsystems in the gas phase (C$^\bullet$ > mC$^\bullet$ > T$^\bullet$), stressing the crucial role of the solvated B-helix environment. The results of our simulations also characterize a more severe distortion for G[8−5]C than for methylene-bridged intrastrand cross-links.

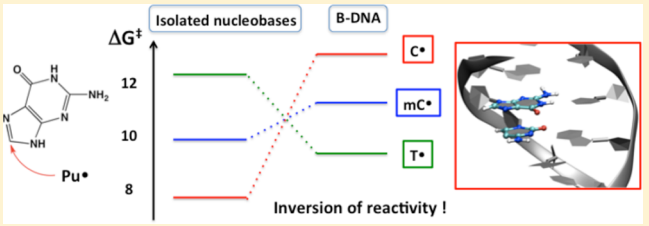

Reactive oxygen species (ROS) continuously trigger chemical modifications to biomolecules, directly or mediated by water. They induce the formation of not only single-nucleobase lesions, which have been extensively studied,[1] but also tandem lesions, which involve two contiguously damaged nucleotides.[2−4] For instance, in 1997, Freund and co-workers evidenced an intrastrand cross-link (ICL) lesion, named G[8−5m]T, in which the methyl carbon atom of thymine is covalently linked to the C8 atom of the adjacent guanine base.[5] Partners other than thymine and guanine can be envisaged. To consider the probability of such a lesion, one has to tackle the ground-state coupling reactivity between the C5 atom of a pyrimidine (either thymine, cytosine, methylcytosine, or uracile) and a neighbor purine base (guanine or adenine, mostly but not exclusively on C8). Furthermore, this reactivity gives rise to two strand orientations.[6] This sketches a large subfamily of lesions, embracing *a priori* 64 oxidative ICLs. Most of them have been intensively characterized in terms of formation yields, mutagenicity, and sometimes thermal destabilization measurements.[7−13] In this rather complicated landscape, the data collected so far delineate some clear tendencies, such as the higher formation yield of G[8−5m]T versus those of T[5m−8]G[14] and G[8−5]C, as well as a lowered reactivity of radical pyrimidines toward adenine.[15] Meanwhile, a few adducts such as C[5−8]G have not yet been detected, even by high-performance mass spectrometry.[11] The quest for these complex lesions is indeed hampered by their rarity, below a threshold of several lesions per 10^8 nucleotides. Measurements of yields of formation have revealed that 0.037 G[8−5]C lesion and 0.050 G[8−5m]T lesion are formed per 10^9 nucleosides and per gray in HeLa-S3 cells,[11] while values for oxidative single-nucleobase lesions are typically 3 orders of magnitude higher.[16]

Among the numerous oxidative ICLs characterized so far, the guanine−cytosine ICL adduct G[8−5]C, in which the C8 atom of the guanine is bonded to the C5 atom of the cytosine, takes on special importance because of its lack of repair.[17,18] In addition, its occurrence is disfavored compared to structurally related methylene-bridged ICLs such as G[8−5m]T.[7,11,19] The formation of G[8−5]C proceeds through the three-step mechanism depicted in Figure 1. It begins (step 1) with the abstraction of the H5 atom of a cytosine,[20,21] which generates in situ a cytosinyl radical. Then (step 2), the cytosinyl radical attacks an adjacent guanine at the C8 position,[22] yielding a G[8−5]C]$^\bullet$ cyclic radical. Finally (step 3), the H8 atom is

Received: September 4, 2012
Revised: December 20, 2012
Published: December 20, 2012

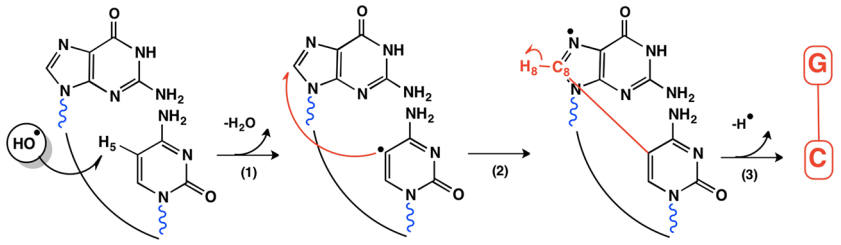

Figure 1. Three-step mechanism for the formation of the G[8−5]C ICL adduct. The key radical attack from C5/H-abstracted cytosine to guanine, on the C8 position, leads to a covalently tethered adduct, displayed with a thick red line. This step (2), the intramolecular addition, is investigated in this study, in a CPMD−QM/MM with frontiers located on the N-glycosidic bonds (blue wavy lines). The choice of a N7-centered radical for the product results from spin density calculations (Figure S3 of the Supporting Information).

removed from the DNA system,[23] restoring a closed-shell species, the G[8−5]C lesion. Note that this mechanism is very similar to that involved in the formation of the closely related G[8−5m]T and G[8−5m]mC (were mC stands for "methyl-cytosine") lesions, for which the initial H abstraction is performed on the Me(C5) group (see, e.g., Figure 1 of ref 24). Cytosine methylation is a common mutation having the specific effect of reducing the level of gene expression. More specifically, it has been reported[19] to increase the level of formation of guanine−(methyl)cytosine ICLs by a factor of 10.

We stress that, as for all other oxidative ICLs, it is currently not possible to isolate experimentally G[8−5]C (or G[8−5m]mC or G[8−5m]T) in a DNA macromolecule and resolve its structure by either nuclear magnetic resonance or X-ray diffraction, yet it is of utmost importance to gain structural insight about this lesion, to improve our ability to repair it. As stated in ref 3, complex lesions are "a matter of debate for more than 40 years due to the lack of accurate methods for (their) measurement". Computational modeling offers a useful alternative to this issue, because one can build the desired lesion *in silico*, as we did in our previous computational investigation of the G[8−5m]T adduct.[24] A complete study of G[8−5]C adduct formation would require the calculation of the probability of the attack of a hydroxyl radical on the H5 atom of the cytosine in a -G-C- motif, and the investigation of all the steps depicted in Figure 1. However, as we already showed in ref 24, one can gain most of the structural information about the lesion by focusing on step 2 only. Indeed, it is during this step that the two bases are brought close together [cyclization process leading to the G[8−5]Py]$^{\bullet}$ (Py = C, mC, or T) intermediate], which is inevitably associated with a significant local distortion. Thus, the main structural effect on the surrounding DNA macromolecule is expected to occur during this step.

In this study, we have modeled step 2 of the formation of G[8−5]C and G[8−5m]mC, following the same strategy as in our previous study of G[8−5m]T.[24] Our approach is based on state-of-the-art quantum mechanics/molecular mechanics (QM/MM) Car−Parrinello molecular dynamics (CPMD) simulations, which provide a realistic description of the solvated DNA environment.[24−29] This method is an interesting alternative for bridging the gap between the experimental view and the theoretical investigations based on gas-phase or implicit solvent models.[30] Recent studies of intrastrand cross-link formation or repair, first light-induced[27] and more recently oxidative ones, guanine−thymine[24,31] and guanine−uracil,[32] have illustrated the benefits of using CPMD−QM/MM approaches. Beyond reactivity, one gains key information concerning the DNA structural distortion associated with the formation of a covalent linkage between two nucleotides on the same strand, initially separated by ∼3.6 Å.

In this paper, we draw a comparison between the formation of G[8−5]C]$^{\bullet}$, G[8−5m]mC]$^{\bullet}$, and G[8−5m]T]$^{\bullet}$. This can be related to the observed relative yields of formation of the corresponding ICLs, namely, G[8−5]C, G[8−5m]mC, and G[8−5m]T, respectively. We show that the intramolecular G ← C$^{\bullet}$ attack is a rather facile process, although it is disfavored compared to methylene-bridged adducts, G[8−5m]T and G[8−5m]mC. Meanwhile, the B-helix undergoes a more pronounced distortion.

METHODOLOGY AND COMPUTATIONAL DETAILS

Our simulation setup is based on the CPMD−QM/MM protocol that we used in our previous study of the G[8−5m]T lesion.[24] Here we briefly summarize the main aspects of this setup and provide more details in the Supporting Information. Our simulations were initiated from the self-complementary model sequence d[AGAGA**G**C**A**GAGT] (·d-[TCTCTCGTCTCA]) depicted in Figure 2. The cytosine

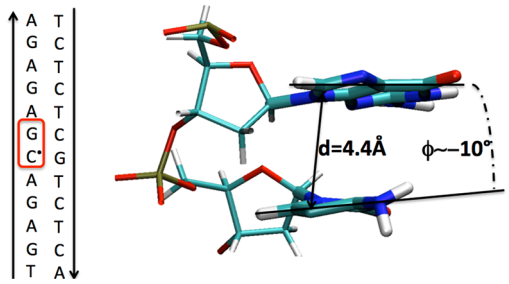

Figure 2. Cartoon representation of the reactive guanine−cytosinyl (or 5-methylcytosinyl) radical moiety, embedded in a fully solvated dodecameric sequence (not displayed). One notes a deplanarization of cytosine after hydrogen abstraction at the C5 position, and a rotation along the N-glycosidic bond captured by a shy plane-to-plane angle deviation of approximately −10°. The approaching distance *d* is consequently increased compared to that of the internucleobase species.

located in the central guanine−cytosine motif (inside the red box in Figure 2) was transformed manually into either a cytosinyl or a 5-methylcytosinyl radical (second structure in Figure 1) to obtain the structure ready to perform step 2. The resulting dodecamer differs from that of ref 24 only by the cytosinyl (or 5-methylcytosinyl) radical and the corresponding G base in the opposite strand and thus allows a more direct comparison between the G[8−5m]T and G[8−5]C (or G[8−5m]mC) lesions.

dx.doi.org/10.1021/bi301198h | *Biochemistry* 2013, 52, 425−431

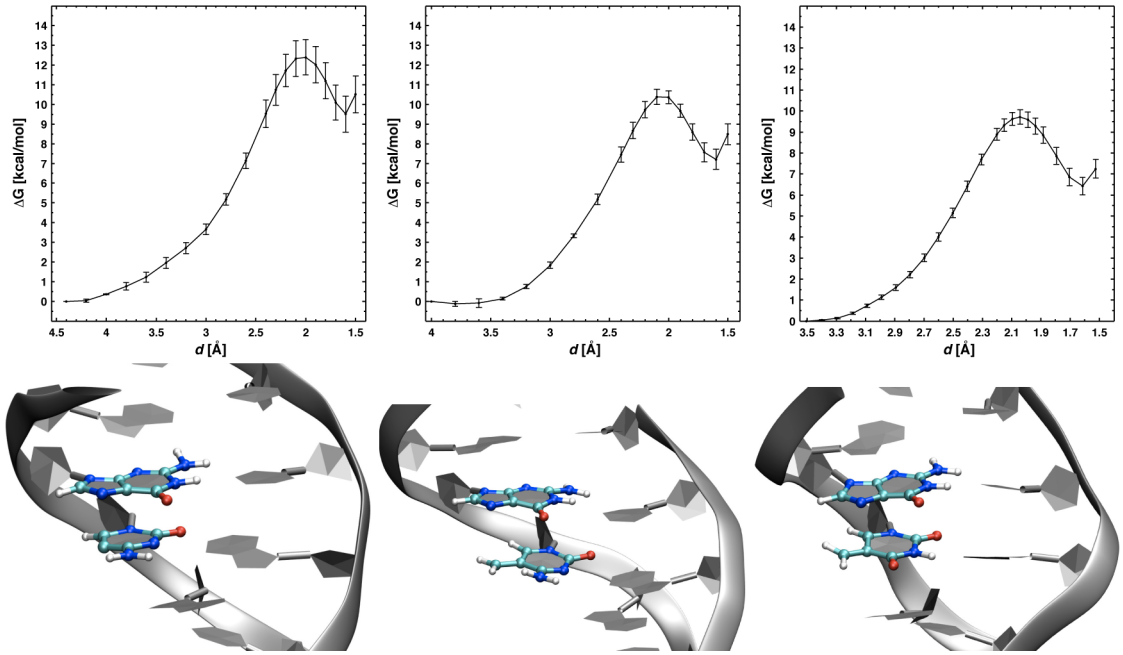

Figure 3. Free energy profiles (top) obtained by thermodynamic integration for the cyclization step in the formation of the G[8−5]C, G[8−5m]mC, and G[8−5m]T lesions (step 2 in Figure 1) and cartoon representations (bottom) for a distance d of 3.6 Å (red dashed line) associated with planarity. The two nucleobases whose atoms are displayed as balls and sticks form the QM part.

After a classical molecular dynamics (MD) equilibration of ∼6 ns using the AMBER99 force field,[33] a low-root-mean-square deviation structure was extracted and taken as a starting structure for QM/MM simulations. The QM part included the two reactive nucleobases, G6 and C7$^{\bullet}$ (or mC7$^{\bullet}$), and was described using DFT with the BLYP functional and the DCACP dispersion correction pseudopotentials, as tested in refs 24 and 34. After an unconstrained CPMD−QM/MM simulation of 2 ps, the reaction coordinate d(G6/C8−C7/C5) was fixed to 4.4 Å and then decreased up to 1.5 Å in a stepwise procedure. The total simulation length was ∼50 ps. The free energy profile along this reaction coordinate was obtained by thermodynamic integration, using the method of constraints.[35] Helical analysis was performed on the fly using 3DNA.[36]

With regard to the possible limits of the model, it should be stressed that QM/MM studies using *ab initio* methods [sometimes termed QM(ai)/MM] usually involve only limited conformational sampling.[37,38] This is due to the fact that the (expensive) evaluation of *ab initio* QM forces over many MD steps still represents a challenge for today's computers. As far as we know, the only method that allows for extensive sampling together with a very good reproduction of free energy barriers of molecular reactions in the condensed phase is the empirical valence bond (EVB).[38,39] The advantage of this approach is that it uses a Hamiltonian whose elements are represented by simple analytic functions that are calibrated over experiments and/or accurate *ab initio* calculations about the reaction in water (see also ref 40 for a discussion). This allows a much faster computation of the forces acting on each atom at each MD step than in QM(ai)/MM calculations. Another promising related method is paradynamics,[41] which involves an EVB Hamiltonian for performing the sampling, and a QM(ai)/MM Hamiltonian for refining the EVB Hamiltonian and computing the free energy barrier.

However, the use of such approaches, which would require a careful parametrization of the EVB Hamiltonian, is outside the scope of this study. Here we assume (like in all previous related studies of DNA-based systems[24−29]) that CPMD−QM/MM simulations of a few picoseconds in each thermodynamic integration window (see the Supporting Information for more details) are sufficient to provide a reasonable description of solvent adaptation around the reacting solute, albeit not fully quantitative.

As a final remark, it is worth noting the AMBER99 force field is known to induce nonphysical distortions of double-stranded DNA on the 100 ns time scale.[42] However, the time scale covered by our simulations is much smaller (∼50 ps in total), and we expect that no such artificial distortion can occur. Here the force field is used, for those parts that are not treated quantum-mechanically, to describe the (mostly harmonic) motions occurring in the subspace that is orthogonal to the reaction coordinate. AMBER 99 has been the force field of choice for many previous studies of DNA-based systems using the same CPMD−QM/MM approach. In particular, severe DNA distortions induced by cyclobutane pyrimidine dimers[27] or by binders[26,43] were elucidated using this force field.

RESULTS AND DISCUSSION

The unconstrained CPMD−QM/MM simulation of the solvated dodecamer featuring a cytosinyl radical prior to the thermodynamic integration procedure reveals that the hydrogen abstraction at C5 (step 1 in Figure 1) has a limited impact on the B-helix structure. A relevant descriptor is angle ϕ formed by the G6 and the C7$^{\bullet}$ planes. A value centered around 0° would indicate that the π-stacking is maintained. Here ϕ is mostly slightly negative, with an average value of approximately −10°. It reflects a shy rotation of cytosine with respect to the N-glycosidic bond, associated with a deplanarization as represented in Figure 2. We note that this deviation remains limited compared to thermal fluctuations (±20°). Consequently, the distance d between the C5 atom of cytosine and the C8 atom of guanine, which constitutes our reaction

dx.doi.org/10.1021/bi301198h | *Biochemistry* 2013, 52, 425−431

Table 1. Relative Energies and Geometrical Characterization of the Three Stationary Points for the Cyclization Step in the Formation of the G[8−5]C, G[8−5m]mC, and G[8−5m]T Lesions (step 2 in Figure 1)[a]

		energetics		structure								
				reactant			transition state			product		
pyrimidine	model	$\Delta G^{\ddagger}$	$\Delta_r G$	d	ϕ	bend	d	ϕ	bend	d	ϕ	bend
C$^{\bullet}$	isolated	9.0	−18.5	3.34	−9.7	–	2.50	103.7	–	1.53	123.4	–
	12 bp	12.4	9.5	4.40	−10.0	7.6	1.95	31.6	11.5	1.50	55.1	24.3
mC$^{\bullet}$	isolated	10.6	3.2	3.21	−7.9	–	2.10	13.4	–	1.61	20.4	–
	12 bp	10.5	8.5	3.60	0.3	5.7	2.10	22.8	5.2	1.50	28.2	10.0
T$^{\bullet}$	isolated	11.8	5.8	3.20	−5.7	–	2.09	9.4	–	1.61	15.5	–
	12 bp	9.7	6.5	3.50	−1.8	4.4	1.90	25.9	15.1	1.50	35.2	20.1

[a]Isolated nucleobases are built to respect the 5′ ← 3′ orientation. Cartoon representations of the G[8−5]C lesion are given in Figure 4.

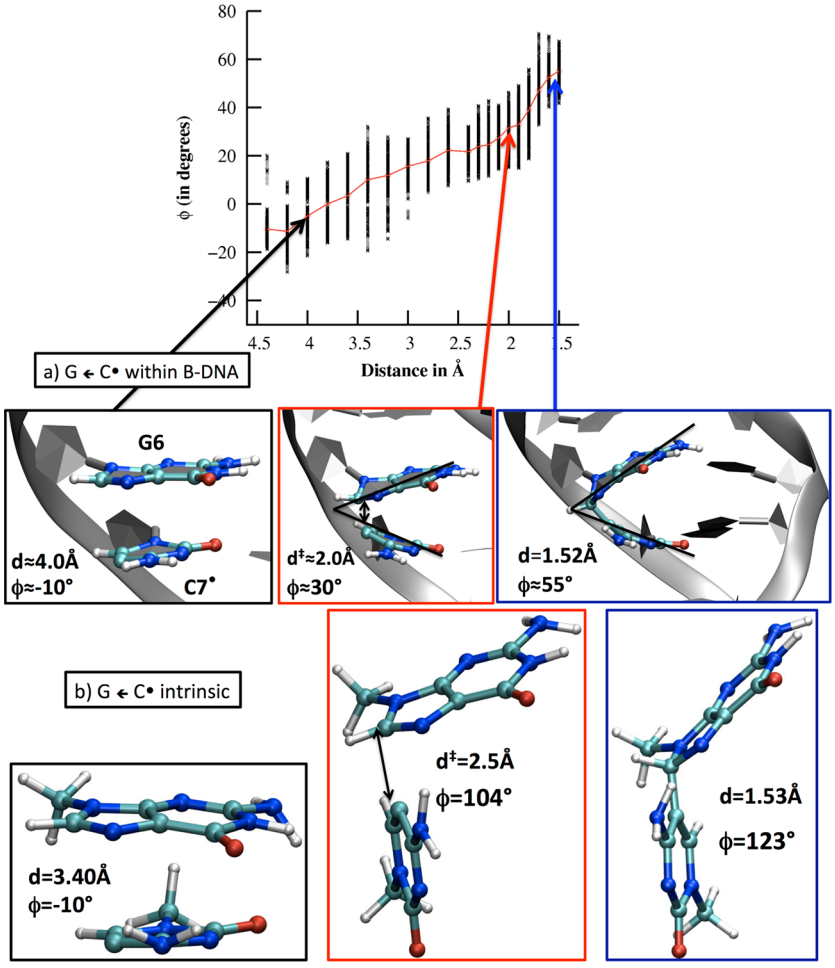

Figure 4. Structural evolution of the guanine−cytosine motif along the reaction coordinate of the cyclization process (step 2 in Figure 1). The lack of conformational flexibility between the base pairs[51] is further reinforced within a B-DNA environment, and the latter thwarts a "destacking" of the linked nucleobases. The last row illustrates the conformational freedom of the isolated base pairs, in contrast with the restriction of the accessible conformations of the product within a helical pattern.

coordinate, is impacted. Our simulations show that d is centered around 4.0 ± 0.3 Å, and hence slightly superior to the initial G6(C8)−T7(Me-C5) distance in the case of the G[8−5m]T lesion (3.6 Å as in ref 24). Meanwhile, the analogue distance between the same C/C5 atom and the C8 atom of adenine A8 fluctuates around 5.5 Å, i.e., systematically greater than d toward G6 (see Figure S2 of the Supporting Information). This is strongly expected to penalize the cyclization of C[5−8]A versus G[8−5]C, following the geometrical argument that a longer approaching distance in the reactant will be associated with a higher activation free energy.[24] This corroborates the fact that the C[5−8]A lesion has never been identified experimentally within oligonucleotides, all the more because adenine is less reactive toward coupling.[14,15,44] Hence, this sequence effect is discarded in this study.

The free energy profile computed for the G ← C$^{\bullet}$ intramolecular addition is plotted in Figure 3. Relevant energetic and structural data are also listed in Table 1. The abscissa d ranges from 4.4 to 1.5 Å along step 2, with a

dx.doi.org/10.1021/bi301198h | Biochemistry 2013, 52, 425−431

transition state located at a $d^{\ddagger}$ of ∼2.0 Å. The latter value is typical for an activation distance for the formation of a carbon−carbon single bond in biological systems.[45] More specifically, we obtain a very similar critical distance $d^{\ddagger}$ for the formation of the G[8−5m]T]$^{\bullet}$ adduct and the analogue guanine−methylcytosyl G[8−5m]mC]$^{\bullet}$ radical. Even if the transition-state distance $d^{\ddagger}$ is similar, the structures of the G···Py]$^{\bullet}$ reactants (Py = C, mC, or T) embedded in the double-helix structure strongly depend on the nature of the radical pyrimidine. In particular, a maintained planarity between G6 and the two later radicals was reported.[24] In turn, the average structure of the reactant presents an angle ϕ of ∼0°. The approaching distance between the guanine and cytosinyl radical is greater by 0.8 Å, which is reflected in the free energy profile: restoring a shorter distance between the nucleobases is associated with a low free energetic penalty of ∼1.2 kcal/mol.

The activation free energies of step 2 of the three oxidative ICL lesions indeed single out the G[8−5]C lesion, with a barrier $\Delta G^{\ddagger}$ estimated to be 12.4 ± 0.9 kcal/mol. The G ← C$^{\bullet}$ cyclization is a rather facile process, although other DNA damages typically occur with an even lower activation free energy. For instance, photolesions are barrierless upon the absorption of UV light,[30] and the two other free energy barriers for radical cyclization onto guanine and C8 are estimated to be 10.5 and 9.7 kcal/mol for methylcytosine and thymine, respectively (see Figure 3). According to the activation barriers obtained from our simulations, we can establish the following reactivity order:

$$T^{\bullet} > mC^{\bullet} > C^{\bullet} \quad (1)$$

All three cyclizations are endergonic processes, with $\Delta_r G$ values of 9.5, 8.5, and 6.5 kcal/mol for C, mC, and T, respectively. These values follow a monotonous yet nonlinear dependence with respect to activation free energies, such that the kinetic and thermodynamic perspectives converge. Our data tend to indicate that the G[8−5m]T and G[8−5]C adducts delineate the two extreme cases of this subfamily of tandem lesions. They provide a quantitative view of the T$^{\bullet}$, mC$^{\bullet}$, and C$^{\bullet}$ positioning toward guanine G6 attack. Cytosine methylation corresponds to a decrease of 2 kcal/mol in the cyclization activation free energy, while the endergonicity is weakened by ∼1 kcal/mol. Radical thymine gives the lowest-energy profile, with an additional decrease of 1 kcal/mol for $\Delta G^{\ddagger}$ and an ∼6 kcal/mol endergonicity. Nevertheless, these energies cannot be related to the experimental yields of formation given in the introductory section; the latter embrace the whole formation pathway and are reported for a specific set of operating conditions, yet our simulations show significant differences in cyclization profiles among the three hydrogen-abstracted pyrimidines. Hence, this step plays a role in easing the formation of methylene-bridged adducts, and not solely initiation of hydrogen abstraction known to be favored on the methyl group of mC compared to C5.[46,47]

The construction of a complete picture with the kinetic data from simulations is the ultimate goal but is outside the scope of this study (see Methodology and Computational Details for a discussion of the limits of the QM/MM approach). It is nevertheless insightful to examine step 2 in more detail and to identify the factors leading to the reactivity order of eq 1. The cyclization profile reflects the intrinsic ease of the radical attack, modulated by a more or less destabilizing contribution arising from the distortion of the B-helix. The first contribution can be assessed by DFT/BLYP-D calculations of free nucleobases (i.e., the same atoms as the QM part used in our QM/MM calculations) in the gas phase. The free energies listed in Table 1 indicate that C$^{\bullet}$ is a more intrinsically efficient tandem partner than 5-methylcytosine and thymine, with an activation barrier ($\Delta G^{\ddagger}$) of 9.0 kcal/mol compared to barriers of 10.6 and 11.8 kcal/mol, respectively. The recently proposed index of radical electrophilicities[48] corroborates this $\Delta G^{\ddagger}$ sequence (see the Supporting Information), which is also in line with the $\Delta_r G$ values that establish the same sequence from a thermodynamic perspective. The reactivity order (C$^{\bullet}$ > mC$^{\bullet}$ > T$^{\bullet}$) obtained in the gas phase is reversed compared to that established within DNA (eq 1), which highlights the decisive contribution from the solvated B-helix environment. A graphical representation is given in Figure 3. This dramatic environment effect can be understood by analyzing the evolutions of the ϕ angle along the reaction coordinate. The d and ϕ values for the transition states and products associated with T$^{\bullet}$ and mC$^{\bullet}$ do not differ significantly between free nucleobases and their counterparts within the DNA double helix. However, for C$^{\bullet}$, deviations are much more pronounced; isolated nucleobases form adducts with an angle of ∼123° (Figure 5, bottom right). Within

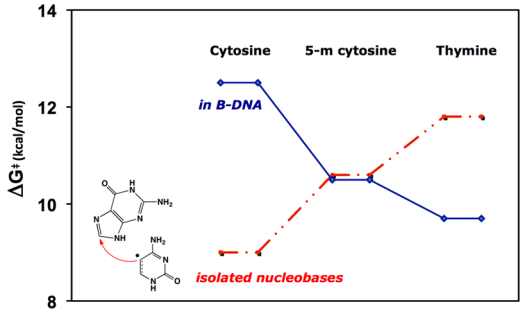

Figure 5. Activation energies for the G ← Py$^{\bullet}$ cyclization (step 2 in Figure 1). The intrinsinc electronic reactivity sequence is reversed as the mechanical embedding of the B-helix comes into play.

double-stranded DNA, ϕ monotonously increases from an initially small negative value at d = 4.4 Å to become clearly positive and fluctuates around 30° in the activated region (d ∼ 2 Å). This increase becomes more steep going to the product, as the system becomes locally rigid, to finally reach ∼55°. This indicates that the conformational freedom from which the free nucleobases benefit is severely restricted within the DNA double helix because of geometrical and steric constraints. The solvated helix restricts the accessible conformations of the guanine−cytosine moiety and destabilizes the linked nucleobases for the transition state and *a fortiori* product structures. This is reflected in the fact that the marked exergenicity for G[8−5]C]$^{\bullet}$ adduct formation ($\Delta_r G$ = −18.5 kcal/mol) is reversed to an endergonicity once the cyclization takes place within B-DNA.

The guanine−cytosinyl radical moeity centered in a dodecamer is strongly influenced by the solvated DNA environment and adopts a restricted conformation that can coexist with both coaxial stacking and Watson−Crick hydrogen bond pairing. The final value of ϕ, which is intermediate between π-stacking and orthogonality, evidences an energetic and structural compromise.

Interestingly, the importance of the embedding is much less marked for the G[8−5m]mC]$^{\bullet}$ and G[8−5]T]$^{\bullet}$ radical adducts. Both present similar values of d and ϕ when isolated and when embedded within B-DNA (Table 1). Furthermore,

dx.doi.org/10.1021/bi301198h | *Biochemistry* 2013, 52, 425−431

the ϕ values for both these lesions are also similar in each of these two cases. Thus, unlike G[8−5]C]•, the intrinsic structure of these adducts can be easily accommodated with B-DNA without invoking any serious steric clashes with neighboring groups. The methylene spacer allows enough flexibility for a π-stacking benefit in all cases, and the plane-to-plane angle is reduced by more than half compared to that of G[8−5]C]• (∼25° for the G[8−5m]T]• and G[8−5m]mC]• radicals).

Beyond the ϕ descriptor, the structural interplay between the G[8−5]C lesion and the macromolecular helix can be more globally characterized by helical analysis.[24] First, the bend angle defined by the normal vectors of the two base steps (Figure S4 of the Supporting Information) stays close to 5−10° up to a distance d of 3 Å and then increases to 25°. This latter value, which corresponds to that of the cyclized adduct, is slighty higher than those obtained for G[8−5m]T]• and G[8−5m]mC]•, 20° and 10°, respectively. The second descriptor is the unwind angle, defined by the difference between twist angles (Figure S4 of the Supporting Information). It presents limited variations, between 6 and 8° and independent of the nature of the pyrimidine radical. Finally, the evolution of the six hydrogen bond distances of the Watson−Crick pairing for G6/C18 and C7/G19 (Figure S5 of the Supporting Information) shows a near stability until the product region is approached (d ∼ 1.7 Å), where the hydrogen bond becomes weakened. Again, this constitutes a common point for the three oxidative guanine−pyridimine lesions, in line with the seminal study by Kishi and co-workers,[49] and contrasts with some photolesions that induce a disruption of the Watson−Crick pairing.[50] Altogether, this generalizes the results obtained for G[8−5m]T,[24] with oxidative ICLs that present smaller deviations compared to photolesions.

CONCLUDING REMARKS

In this study, state-of-the-art simulations were used to gain insights into the formation of the guanine−cytosine ICLs (G[8−5]C and G[8−5m]mC) inside a DNA dodecamer. Following the philosophy of our previous investigation of the guanine−thymine (G[8−5m]T) ICL,[24] we focused on the second step in the reaction because it is during this step that cyclization occurs, and this cyclization is expected to have the most important impact on the global structure of the DNA macromolecule. This reaction turns out to be particularly sensitive to environmental effects. We have illustrated the interplay between the geometry of the cyclized G[8−5]C]• (or G[8−5m]mC]•) intermediate (measured by angle ϕ formed by the guanine and the cytosine planes) and the global structure of the DNA dodecamer (measured by twist, bend, roll, and tilt angles) in which the reaction takes place. While the cytosinyl radical has an intrinsically higher reactivity (in gas phase) than the thyminyl radical against guanine, the B-DNA environment reverses this reactivity order. We have shown that methylene-bridged ICLs such as G[8−5m]T or G[8−5m]mC lesions are better accommodated in the B-DNA framework than those that do not contain the methylene bridge such as the G[8−5]C lesion. Our results indicate that this methylene group acts as a spacer that helps the cyclization process: the G[8−5m]mC]• and G[8−5m]T]• intermediates are typically more flexible and loose than the G[8−5]C]• intermediate.

ASSOCIATED CONTENT

Supporting Information

Full methodological details concerning the classical and QM/MM dynamics, overall root-mean-square deviation of the C7/hydrogen-abstracted dodecamer and time evolution of ϕ and d along the classical trajectory, helical analysis along the reaction pathway with evolution of the rool, tilt, bend, and twist angles, time evolution of the six Watson−Crick hydrogen bonds around G6·C18 and C7·G19 base pairs along the reaction path, and radical electrophilicity indices (as defined in ref 48, conceptual DFT) for radical pyrimidines. This material is available free of charge via the Internet at http://pubs.acs.org.

AUTHOR INFORMATION

Corresponding Author

*E-mail: elise.dumont@ens-lyon.fr. Phone: +33 4 72 72 88 46. Fax: +33 4 72 72 88 60.

Funding

C.P. is grateful for a Ph.D. fellowship from the French Ministery of research. This work is supported by the Labex PRIMES (ANR contract).

Notes

The authors declare no competing financial interest.

ACKNOWLEDGMENTS

Calculations were performed using the local HPC resources of PSMN/Centre Blaise Pascal at ENS-Lyon.

REFERENCES

(1) Kanvah, S., Joseph, J., Schuster, G. B., Barnett, R. N., Ceveland, C. L., and Landman, U. (2010) Oxidation of DNA: Damage to Nucleobases. *Acc. Chem. Res. 43*, 280−287.

(2) Cadet, J., Ravanat, J.-L., Taverna-Porro, M., Menoni, H., and Angelov, D. (2012) Oxidatively generated complex DNA damage: Tandem and clustered lesions. *Cancer Lett. 327*, 5−15.

(3) Cadet, J., Douki, T., and Ravanat, J.-L. (2010) Oxidatively generated base damage to cellular DNA. *Free Radical Biol. Med. 49*, 9−21.

(4) Bergeron, F., Auvre, F., Radicella, J. P., and Ravanat, J.-L. (2010) HO• radicals induce an unexpected high proportion of tandem base lesions refractory to repair by DNA glycosylases. *Proc. Natl. Acad. Sci. U.S.A. 107*, 5528−5533.

(5) Box, H. C., Budzinski, E. E., Dawidzik, J. B., Gobey, J. S., and Freund, H. G. (1997) Free Radical-Induced Tandem Base Damage in DNA Oligomers. *Free Radical Biol. Med. 23*, 1021−1030.

(6) Hong, H., and Wang, Y. (2005) Formation of Intrastrand Cross-Link Products between Cytosine and Adenine from UV Irradiation of d(BrCA) and Duplex DNA Containing a 5-Bromocytosine. *J. Am. Chem. Soc. 127*, 13969−13977.

(7) Gu, C., and Wang, Y. (2005) Thermodynamic and in Vitro Replication Studies of an Intrastrand G[8−5]C Cross-Link Lesion. *Biochemistry 44*, 8883−8889.

(8) Zeng, Y., and Wang, Y. (2006) Sequence-dependent formation of intrastrand crosslink products from the UVB irradiation of duplex DNA containing a 5-bromo-2′-deoxyuridine or 5-bromo-2′-deoxycytidine. *Nucleic Acids Res. 34*, 6521−6529.

(9) Gu, C., Zhang, Q., Yang, Z., Wang, Y., Zhou, Y., and Wang, Y. (2006) Recognition and incision of oxidative intrastrand cross-link lesions by UvrABC nuclease. *Biochemistry 45*, 10739−10746.

(10) Zeng, Y., and Wang, Y. (2007) UVB-Induced formation of intrastrand cross-link products of DNA in MCF-7 cells treated with 5-bromo-2′-deoxyuridine. *Biochemistry 46*, 8189−8195.

(11) Hong, H., Cao, H., and Wang, Y. (2007) Formation and genotoxicity of a guanine-cytosine intrastrand cross-link lesion in vivo. *Nucleic Acids Res. 35*, 7118−7127.

(12) Jiang, Y., Wang, Y., and Wang, Y. (2009) In Vitro Replication and Repair Studies of Tandem Lesions Containing Neighboring Thymidine Glycol and 8-Oxo-7,8-dihydro-2′-deoxyguanosine. *Chem. Res. Toxicol. 22*, 574−583.
(13) Lin, G., Zhang, J., Zeng, Y., Luo, H., and Wang, Y. (2010) Conformation-dependent Formation of the G[8−5]U Intrastrand Cross-link in 5-Bromouracil-containing G-quadruplex DNA Induced by UVA Irradiation. *Biochemistry 49*, 2346−2350.
(14) Labet, V., Morell, C., Grand, A., Cadet, J., Cimino, P., and Barone, V. (2008) Formation of cross-linked adducts between guanine and thymine mediated by hydroxyl radical and one-electron oxidation: A theoretical study. *Org. Biomol. Chem. 6*, 3300−3305.
(15) Bellon, S., Ravanat, J.-L., Gasparutto, D., and Cadet, J. (2002) Cross-linked thymine-purine base tandem lesions: Synthesis, characterization, and measurement in γ-irradiated isolated DNA. *Chem. Res. Toxicol. 15*, 598−606.
(16) Kriker, M. C., and Drake, J. W. (1990) Heat mutagenesis in bacteriophage T4: Another walk down the transversion pathway. *J. Bacteriol. 172*, 3037−3039.
(17) Gu, C., and Wang, Y. (2004) LC-MS/MS Identification and Yeast Polymerase η Bypass of a Novel γ-Irradiation-Induced Intrastrand Cross-Link Lesion G[8−5]C. *Biochemistry 43*, 6745−6750.
(18) Wang, J., Cao, H., You, C., Yuan, B., Bahde, R., Gupta, S., Nishigori, C., Niedernhofer, L. J., Brooks, P. J., and Wang, Y. (2012) Endogenous formation and repair of oxidatively induced G[8Sm]T intrastrand cross-link lesion. *Nucleic Acids Res. 40*, 7368−7374.
(19) Cao, H., and Wang, Y. (2007) Quantification of oxidative single-base and intrastrand cross-link lesions in unmethylated and CpG-methylated DNA induced by Fenton-type reagents. *Nucleic Acids Res. 35*, 4833−4844.
(20) Balasubramanian, B., Pogozelski, W. K., and Tullius, T. D. (1998) DNA strand breaking by the hydroxyl radical is governed by the accessible surface areas of the hydrogen atoms of the DNA backbone. *Proc. Natl. Acad. Sci. U.S.A. 343*, 9738−9743.
(21) Aydogan, B., Bolch, W. E., Swarts, S. G., Turner, J. E., and Marshall, D. T. (2008) Monte Carlo Simulations of Site-Specific Radical Attack to DNA Bases. *Radiat. Res. 169*, 223−231.
(22) Chatgilialoglu, C., Caminal, C., and Mulazzani, Q. G. (2011) Radical-based alkylation of guanine derivatives in aqueous medium. *Org. Biomol. Chem. 9*, 3494−3498.
(23) Hong, I. S., Carter, K. N., Sato, K., and Greenberg, M. M. (2007) Characterization and mechanism of formation of tandem lesions in DNA by a nucleobase peroxyl radical. *J. Am. Chem. Soc. 129*, 4089−4098.
(24) Garrec, J., Patel, C., Rothlisberger, U., and Dumont, E. (2012) Insights into Intrastrand Cross-Link Lesions of DNA from QM/MM Molecular Dynamics Simulations. *J. Am. Chem. Soc. 134*, 2111−2119.
(25) Stevens, K., Claeys, D. D., Catak, S., Figaroli, S., Hocek, M., Tromp, J. M., Schurch, S., Van Speybroeck, V., and Madder, A. (2011) Furan-Oxidation-Triggered Inducible DNA Cross-Linking: Acyclic Versus Cyclic Furan-Containing Building Blocks—On the Benefit of Restoring the Cyclic Sugar Backbone. *Chem.—Eur. J. 17*, 6940−6953.
(26) Gossens, C., Tavernelli, I., and Rothlisberger, U. (2008) DNA Structural Distortions Induced by Ruthenium-Arene Anticancer Compounds. *J. Am. Chem. Soc. 130*, 10921−10928.
(27) Masson, F., Laino, T., Tavernello, I., Rothlisberger, U., and Hutter, J. (2008) Computational Study of Thymine Dimer Radical Anion Splitting in the Self-Repair Process of Duplex DNA. *J. Am. Chem. Soc. 130*, 3443−3450.
(28) Ceron-Carrasco, J. P., Zuniga, J., Requena, A., Perpete, E. A., Michaux, C., and Jacquemin, D. (2011) Combined effect of stacking and solvation on the spontaneous mutation in DNA. *Phys. Chem. Chem. Phys. 13*, 14584−14589.
(29) Loos, P.-F., Dumont, E., Laurent, A. D., and Assfeld, X. (2009) Important effects of neighbouring nucleotides on electron induced DNA single-strand breaks. *Chem. Phys. Lett. 475*, 120−123.
(30) Durbeej, B., and Eriksson, L. A. (2003) On the Formation of Cyclobutane Pyrimidine Dimers in UV-irradiated DNA: Why are Thymines More Reactive ? *Photochem. Photobiol. 78*, 159−167.
(31) Ding, S., Kropachev, K., Cai, Y., Kolbanovskiy, M., Durandina, S. A., Liu, Z., Shafirovich, V., Broyde, S., and Geacintov, N. E. (2012) Structural, energetic and dynamic properties of guanine(C8)-thymine-(N3) cross-links in DNA provide insights on susceptibility to nucleotide excision repair. *Nucleic Acids Res. 40*, 2059−2517.
(32) Churchill, C. D. M., Eriksson, L. A., and Wetmore, S. D. (2011) Formation Mechanism and Structure of a Guanine-Uracil DNA Intrastrand Cross-Link. *Chem. Res. Toxicol. 24*, 2189−2199.
(33) Wang, J., Cieplak, P., and Kollman, P. A. (2000) How well does a restrained electrostatic potential (RESP) model perform in calculating conformational energies of organic and biological molecules? *J. Comput. Chem. 21*, 1049−1074.
(34) Dupont, C., Patel, C., and Dumont, E. (2011) Improved DFT Description of Intrastrand Cross-Link Formation by Inclusion of London Dispersion Corrections. *J. Phys. Chem. B 115*, 15138−15144.
(35) Sprik, M., and Ciccotti, G. (1998) Free energy from constrained molecular dynamics. *J. Chem. Phys. 109*, 7737−7744.
(36) Lu, X.-J., and Olson, W. K. (2008) 3DNA: A versatile, integrated software system for the analysis, rebuilding and visualization of three-dimensional nucleic-acid structures. *Nat. Protoc. 3*, 1213−1227.
(37) Kamerlin, S. C. L., Haranczyk, M., and Warshel, A. (2009) Progress in Ab Initio QM/MM Free-Energy Simulations of Electrostatic Energies in Proteins: Accelerated QM/MM Studies of pKa, Redox Reactions and Solvation Free Energies. *J. Phys. Chem. B 113*, 1253−1272.
(38) Kamerlin, S. C. L., and Warshel, A. (2010) The EVB as a quantitative tool for formulating simulations and analyzing biological and chemical reactions. *Faraday Discuss. 145*, 71−106.
(39) Warshel, A., and Weiss, R. M. (1980) An empirical valence bond approach for comparing reactions in solutions and in enzymes. *J. Am. Chem. Soc. 102*, 6218−6226.
(40) Garrec, J., Sautet, P., and Fleurat-Lessard, P. (2011) Understanding the HIV-1 Protease Reactivity with DFT: What Do We Gain from Recent Functionals? *J. Phys. Chem. B 115*, 8545−8558.
(41) Plotnikov, N. V., and Warshel, A. (2012) Exploring, Refining, and Validating the Paradynamics QM/MM Sampling. *J. Phys. Chem. B 116*, 10342−10356.
(42) Perez, A., Marchan, I., Svozil, D., Sponer, J., Cheatham, T. E., III, Laughton, C. A., and Orozco, M. (2007) Refinement of the AMBER Force Field for Nucleic Acids: Improving the Description of α/γ Conformers. *Biophys. J. 92*, 3817−3829.
(43) Vargiu, A. V., Ruggerone, P., Magistrato, A., and Carloni, P. (2008) Dissociation of minor groove binders from DNA: Insights from metadynamics simulations. *Nucleic Acids Res. 36*, 5910−5921.
(44) Xerri, B., Morell, C., Grand, A., Cadet, J., Cimino, P., and Barone, V. (2006) Radiation-induced formation of DNA intrastrand crosslinks between thymine and adenine bases: A theoretical approach. *Org. Biomol. Chem. 4*, 3986−3992.
(45) Himo, F. (2005) C-C bond formation and cleavage in radical enzymes, a theoretical perspective. *Biochim. Biophys. Acta 1*, 24−33.
(46) Wang, W., Jin, L., Wang, W., Lu, J., and Yang, J. (2007) Theoretical study on the multi-channel reaction of OH radical with 5-methylcytosine. *Chem. Phys. Lett. 444*, 359−365.
(47) Luo, Q., Li, J., Li, Q. S., Kim, S., Wheeler, S. E., Xie, Y., and Schaefer, H. F., III (2005) Electron affinities of the radicals derived from cytosine. *Phys. Chem. Chem. Phys. 7*, 861−865.
(48) De Vleeschouwer, F., Geerlings, P., and De Proft, F. (2012) Radical electrophilicities in solvent. *Theor. Chim. Acta 131*, 1−13.
(49) Qiao, X., and Kishi, Y. (1999) Covalently Cross-Linked Watson-Crick Base Pair Models. *Angew. Chem., Int. Ed. 38*, 928−931.
(50) Lee, J.-H., Bae, S.-H., and Choi, B.-S. (2000) The Dewar photoproduct of thymidylyl(3′-5′)-thymidine (Dewar product) exhibits mutagenic behavior in accordance with the "A rule". *Proc. Natl. Acad. Sci. U.S.A. 97*, 4591−4596.
(51) Qiu, Y.-L., Li, H.-Y., Topalov, G., and Kishi, Y. (2000) Covalently cross-linked Watson-Crick base pair models. Part 2. *Tetrahedron Lett. 41*, 9425−9429.